

Cascading Failures as Continuous Phase-Space Transitions

Yang Yang¹ and Adilson E. Motter^{1,2}

¹*Department of Physics and Astronomy, Northwestern University, Evanston, IL 60208, USA*

²*Northwestern Institute on Complex Systems, Northwestern University, Evanston, IL 60208, USA*

In network systems, a local perturbation can amplify as it propagates, potentially leading to a large-scale cascading failure. Here we derive a continuous model to advance our understanding of cascading failures in power-grid networks. The model accounts for both the failure of transmission lines *and* the desynchronization of power generators, and incorporates the transient dynamics between successive steps of the cascade. In this framework, we show that a cascade event is a phase-space transition from an equilibrium state with high energy to an equilibrium state with lower energy, which can be suitably described in closed form using a global Hamiltonian-like function. From this function we show that a perturbed system cannot always reach the equilibrium state predicted by quasi-steady-state cascade models, which would correspond to a reduced number of failures, and may instead undergo a larger cascade. We also show that in the presence of two or more perturbations, the outcome depends strongly on the order and timing of the individual perturbations. These results offer new insights into the current understanding of cascading dynamics, with potential implications for control interventions.

Cascading processes underlie a myriad of network phenomena [1], including blackouts in power systems [2, 3], secondary extinctions in ecosystems [4, 5], and complex contagion in financial networks [6, 7]. In all such cases, an otherwise small perturbation may propagate and eventually cause a sizable portion of the system to fail. Various system-independent cascade models have been proposed [8–13] and used to draw general conclusions, such as on the impact of interdependencies [14] and countermeasures [15]. There are outstanding questions, however, for which it is necessary to model the cascade dynamics starting from the actual dynamical state of the system.

In power-grid networks, the state of the system is determined by the power flow over transmission lines and the frequency of the power generators, which must be respectively below capacity and synchronized under normal steady-state conditions. Although a local perturbation has a limited impact on the connectivity of the network, it may trigger a cascade of failures and protective responses that switch off grid components and may also lead generators to lose synchrony. Much of our current understanding about this process has been derived from quasi-steady-state cascade models [16–21], which use iterative procedures to model the successive inactivation of network components caused by power flow redistributions, while omitting the transient dynamics between steady states as well as the dynamics of the generators. Further understanding has resulted from stability studies focused on the synchronization dynamics of power generators in the absence of flow redistributions [22–26].

Yet, to date no theoretical approach has been developed to incorporate at the same time these two fundamental aspects of power-grid dynamics—frequency change and flow redistribution—in the modeling of cascading failures [27]. The goal of our study is to fill this gap and consider the interaction between these two factors. Our framework is inspired by energy function anal-

ysis approaches considered in the study of power system stability [28, 29] and of bistability of circuit elements [30].

Specifically, in this Letter we introduce a time-continuous cascade model that includes the dynamics of the state variables—governed by the swing equations of the generators, frequency dependence of loads, and power flow equations—as well as the dynamics of the status variables describing the on/off (i.e., operational/disabled) condition of the transmission lines. Within this model, the steady operating states of the system correspond to stable equilibria, and a cascade event is a phase-space transition from one stable equilibrium to another. We study these states and show that the stable equilibria are the local minima of an energylike function. This leads to numerous important implications that have not been systematically studied before. In particular, it follows from the properties of this function that a perturbed system cannot always reach the equilibrium state predicted by quasi-steady-state models, and may instead approach an equilibrium corresponding to a larger cascade; this highlights the importance of the dynamics between successive steps of a cascade, as considered in our continuous model, which is a factor that has remained unexplored with few exceptions [1, 31–33]. It also follows that the equilibrium energy does not depend monotonically on the number of failures, and that cascades triggered by multiple perturbations depend strongly on the perturbation order. These results suggest the possibility of cascade mitigation using judiciously designed perturbations to steer the system to a preferred equilibrium that would not be reached spontaneously.

We first consider the protective operation, common to most power networks, that *removes* a transmission line when the flow on it exceeds its capacity. We associate each line ℓ with a continuous variable η_ℓ representing its on/off status (as well as the continuous process of switching between the two conditions) and a parameter

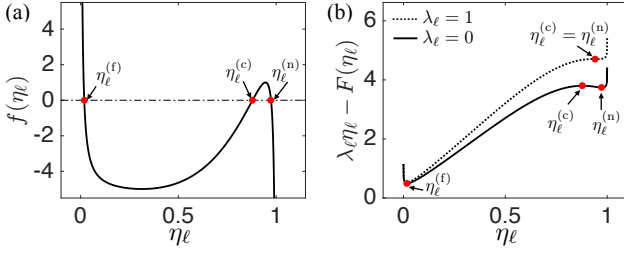


Figure 1. Line-status switch model. (a) Function $f(\eta_\ell)$ for $a = 10$, whose roots are the equilibrium points of Eq. (1) when $\lambda_\ell = 0$ (for other values of λ_ℓ , see Fig. S1 in Supplemental Material [34]). (b) Potential function $\phi(\eta_\ell) = \lambda_\ell \eta_\ell - F(\eta_\ell)$, where the local minima for $\lambda_\ell = 0$ correspond to the stable equilibria in (a). When λ_ℓ is increased past 1, the local minimum $\eta_\ell^{(n)}$ merges with $\eta_\ell^{(c)}$ and then disappears.

λ_ℓ indicating the fraction of the line capacity used by the flow. As shown below, this allows us to incorporate the line status into the dynamical equations by scaling the power flow terms by η_ℓ , with η_ℓ representing the normal status for $\lambda_\ell < 1$ and the failed status for $\lambda_\ell \geq 1$, where η_ℓ is thus constrained to the unit interval. To model the automatic removal of the overloaded lines, we can then define the dynamics of η_ℓ as

$$\dot{\eta}_\ell = f(\eta_\ell) - \lambda_\ell, \quad (1)$$

where the rhs is defined to satisfy three physical conditions: (I) for $\lambda_\ell < 1$, there are three equilibria $\eta_\ell^{(f)} < \eta_\ell^{(c)} < \eta_\ell^{(n)}$, where $\eta_\ell^{(n)} \approx 1$ is a stable equilibrium representing the normal operation status, $\eta_\ell^{(f)} \approx 0$ is a stable equilibrium representing the failed status, and $\eta_\ell^{(c)}$ is an unstable equilibrium marking the critical value below which η_ℓ evolves to the failed status; (II) for $\lambda_\ell \geq 1$, only the equilibrium $\eta_\ell^{(f)}$ remains stable, which is satisfied if the local maximum of f in $(\eta_\ell^{(c)}, \eta_\ell^{(n)})$ is 1; (III) $\eta_\ell^{(c)}$ is always close to 1, since a line should be fully operational under normal conditions. The dynamics does not depend sensitively on the details of function f provided these conditions are satisfied. Throughout, we use overdot to indicate time derivative.

Here we define $f(\eta_\ell) = a^{-1}[\eta_\ell^{-1} - (1 - \eta_\ell)^{-1}] + a\eta_\ell^4 - b$, where a and b are positive parameters. The terms η_ℓ^{-1} and $-(1 - \eta_\ell)^{-1}$ constrain η_ℓ above 0 and below 1, re-

spectively, as they ensure that $f(\eta_\ell) \rightarrow \infty$ for $\eta_\ell \rightarrow 0^+$ and $f(\eta_\ell) \rightarrow -\infty$ for $\eta_\ell \rightarrow 1^-$. The term η_ℓ^4 allows f to have three roots—corresponding to $\eta_\ell^{(f)}$, $\eta_\ell^{(c)}$, and $\eta_\ell^{(n)}$ for $\lambda_\ell = 0$, as shown in Fig. 1(a). The parameters a and b are adjustable to set $\eta_\ell^{(f)}$ close to 0, to set $\eta_\ell^{(c)}$ and $\eta_\ell^{(n)}$ sufficiently close to 1, and to set the local maximum of f to 1. For this choice of function f , Eq. (1) satisfies conditions (I)-(III). Moreover, the equation can be rewritten as a gradient system $\dot{\eta}_\ell = -d\phi(\eta_\ell)/d\eta_\ell$, where $\phi(\eta_\ell) = \lambda_\ell \eta_\ell - F(\eta_\ell)$, and $dF(\eta_\ell)/d\eta_\ell = f(\eta_\ell)$. As shown in Fig. 1(b), the stable equilibria of this system correspond to the local minima of $\phi(\eta_\ell)$.

Following a perturbation, the power flowing on transmission lines can change dynamically. When the flow on line ℓ reaches its capacity ($\lambda_\ell \geq 1$), the system will experience a saddle-node bifurcation and the status variable η_ℓ will evolve to the stable equilibrium $\eta_\ell^{(f)}$, representing a line switch-off operation. This is a one-way action, since the equilibrium $\eta_\ell^{(f)}$ is stable for any value of λ_ℓ .

Having defined the dynamics of the status variables, we now incorporate the system's protective response into the dynamical equations governing the state of the network. In a network of n nongenerator nodes, each such node is an electric point where power is extracted by a load, received from generators, and/or redistributed among transmission lines. We denote by n_g the number of generators, and by n_l the number of transmission lines. To proceed, we consider the extended representation of the network [37] in which each generator is now an additional node connected to the network through a virtual line (not included in n_l and not subject to failure), leading to a network of $n + n_g$ nodes. For notational convenience, we reindex the generators as the first n_g nodes.

Assuming that the voltage satisfies $|V_i| \approx 1$ (in per unit) for all nodes and that no real power is lost on transmission lines, we can define the state of a power system as $\mathbf{x} = (\boldsymbol{\omega}, \boldsymbol{\delta}, \boldsymbol{\eta})$. Here, $\boldsymbol{\omega} = (\omega_i)$ are the frequencies of the generators relative to the system's nominal frequency, $\boldsymbol{\delta} = (\delta_i)$ are the phase angles of all other nodes relative to a reference node (taken to be $i = 1$, so that $\delta_1 \equiv 0$), and $\boldsymbol{\eta} = (\eta_\ell)$ are the status variables of the (nonvirtual) transmission lines \mathcal{L} , where $\ell \in \mathcal{L}$. The state of the system is suitably determined by the following equations:

$$\begin{aligned} \dot{\omega}_i &= -\frac{D_i}{M_i} \omega_i - \frac{1}{M_i} \left[P_i + \sum_{j=n_g+1}^{n_g+n} \tilde{B}_{ij} \sin \delta_{ij} \right], & i = 1, 2, \dots, n_g, \\ \dot{\delta}_i &= \omega_i - \omega_1, & i = 2, \dots, n_g, \\ \dot{\delta}_i &= -\frac{1}{T_i} \left[P_i + \sum_{j=1}^{n_g} \tilde{B}_{ij} \sin \delta_{ij} + \sum_{j=n_g+1}^{n_g+n} \tilde{B}_{ij} \eta_{\ell_{i-j}} \sin \delta_{ij} \right] - \omega_1, & i = n_g + 1, \dots, n_g + n, \\ \dot{\eta}_{\ell_{i-j}} &= 10 \left[f(\eta_{\ell_{i-j}}) - \frac{\tilde{B}_{ij} (1 - \cos \delta_{ij})}{W_{\ell_{i-j}}} \right], & \ell_{i-j} \in \mathcal{L}. \end{aligned} \quad (2)$$

Here, $\delta_{ij} = \delta_i - \delta_j$ and \tilde{B} is a symmetric matrix with nonzero elements $\tilde{B}_{ij} = -1/x_{\ell_{i-j}}$, where $x_{\ell_{i-j}}$ is the transient reactance of a generator or is the reactance of a transmission line, depending on whether the line connecting i and j is virtual or not. The first two equations are the swing equations describing the dynamics of the generators, where M_i is the generator rotor inertia, D_i is the rotor damping ratio, and P_i is the negative of the mechanical power input $P_i^{(m)}$ of the generator [38]. The third equation describes loads (and nongenerator nodes in general, under the assumption that they include some frequency-dependent power exchange) as first-order rotors, where T_i is the load frequency ratio and P_i is the power $P_i^{(d)}$ demanded at the node. We further assume that $\sum_{i=1}^{n_g+n} P_i = 0$, so that there exists an equilibrium point at $\omega_i = 0$ and $\delta_i = cte$. Note that the term representing the power flow on line ℓ_{i-j} is multiplied by the status variable $\eta_{\ell_{i-j}}$, which automatically turns off the line in the event of an overload (when $\eta_{\ell} \rightarrow \eta_{\ell}^{(f)}$). The last equation describes the dynamics of the status variables, where $\lambda_{\ell_{i-j}}$ in Eq. (1) is replaced by $\tilde{B}_{ij}(1 - \cos \delta_{ij})$, the reactance energy stored in the transmission line ℓ_{i-j} , divided by $W_{\ell_{i-j}}$, the maximum reactance energy that line ℓ_{i-j} can hold. The prefactor 10 in this equation assures that the time scale for line failures is much shorter than that of the other dynamical changes in the network. For more details on the derivation of Eq. (2), see Supplemental Material [34].

Importantly, we can show that Eq. (2) can be derived from a Hamiltonian-like system of the form

$$\dot{\mathbf{x}} = J\nabla\Psi(\mathbf{x}), \quad (3)$$

where $\Psi(\mathbf{x})$ is an energy function defined as

$$\begin{aligned} \Psi(\mathbf{x}) = & \sum_{i=1}^{n_g} \left[\frac{1}{2} M_i \omega_i^2 + \sum_{j=n_g+1}^{n_g+n} \tilde{B}_{ij} (1 - \cos \delta_{ij}) \right] \\ & + \sum_{i=n_g+1}^{n_g+n} \sum_{j=i+1}^{n_g+n} \tilde{B}_{ij} (1 - \cos \delta_{ij}) \eta_{\ell_{i-j}} \\ & + \sum_{i=2}^{n_g+n} P_i \delta_i - \sum_{\ell_{i-j} \in \mathcal{L}} W_{\ell_{i-j}} F(\eta_{\ell_{i-j}}), \end{aligned} \quad (4)$$

and J is a matrix of the form

$$J = \begin{bmatrix} J_{11} & J_{12} & J_{13} & \mathbf{0} \\ -J_{12}^T & \mathbf{0} & \mathbf{0} & \mathbf{0} \\ -J_{13}^T & \mathbf{0} & J_{33} & \mathbf{0} \\ \mathbf{0} & \mathbf{0} & \mathbf{0} & J_{44} \end{bmatrix}. \quad (5)$$

In this matrix, the off-diagonal blocks are

$$J_{12} = \begin{bmatrix} \frac{1}{M_1} & \frac{1}{M_1} & \cdots & \frac{1}{M_1} \\ \frac{-1}{M_2} & 0 & \cdots & 0 \\ 0 & \frac{-1}{M_3} & \cdots & 0 \\ \vdots & \vdots & \ddots & \vdots \\ 0 & 0 & \cdots & \frac{-1}{M_{n_g}} \end{bmatrix}, \quad J_{13} = \begin{bmatrix} \frac{1}{M_1} & \cdots & \frac{1}{M_1} \\ 0 & \cdots & 0 \\ \vdots & \vdots & \vdots \\ 0 & \cdots & 0 \end{bmatrix}, \quad (6)$$

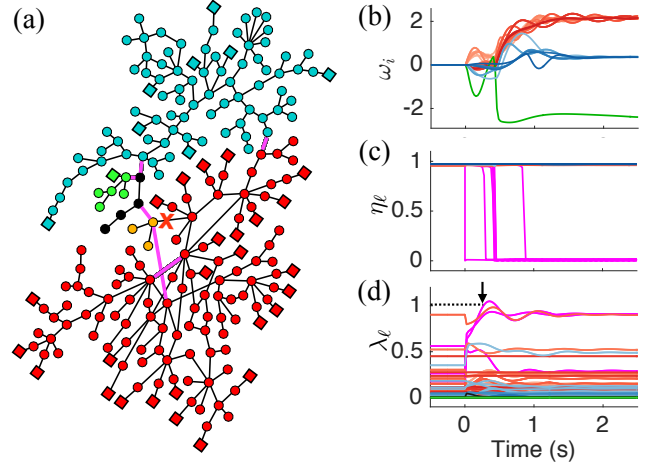


Figure 2. Simulated cascade event in Iceland's power grid. (a) Diagram of the network, which consists of 35 generators (\square), 189 nongenerator nodes (\circ), and 203 transmission lines ($-$) [40]. The removal of the marked line (\times) triggers a sequence of 6 subsequent line failures (magenta) that separate the network into 5 clusters (color coded). (b-c) Corresponding generator frequencies ω_i (b) and line-status variables η_{ℓ} (c) as functions of time [color coded as in (a)]. (d) Corresponding fraction λ_{ℓ} of the line capacity used, should the line overloaded at 0.2 s (arrow) not be disabled.

and the diagonal blocks are

$$\begin{aligned} J_{11} &= \text{diag}\left(-\frac{M_1}{D_1^2}, -\frac{M_2}{D_2^2}, \dots, -\frac{M_{n_g}}{D_{n_g}^2}\right), \\ J_{33} &= \text{diag}\left(-\frac{1}{T_{n_g+1}}, -\frac{1}{T_{n_g+2}}, \dots, -\frac{1}{T_{n_g+n}}\right), \\ J_{44} &= 10 \times \text{diag}\left(-\frac{1}{W_1}, -\frac{1}{W_2}, \dots, -\frac{1}{W_{n_l}}\right). \end{aligned} \quad (7)$$

For details on the derivation of Eq. (3), see Supplemental Material [34].

Crucially, the matrix J is the sum of a skew-symmetric matrix and a diagonal matrix with nonpositive elements, from which we can show that $d\Psi(\mathbf{x}(t))/dt = \nabla\Psi(\mathbf{x})^T \dot{\mathbf{x}} = \nabla\Psi(\mathbf{x})^T J\nabla\Psi(\mathbf{x}) \leq 0$. Moreover, because J is also full rank (which follows from its reduced row echelon form), we have that $d\Psi(\mathbf{x}(t))/dt = \mathbf{0}$ if and only if $\nabla\Psi(\mathbf{x}) = \mathbf{0}$, and hence if and only if $\dot{\mathbf{x}} = J\nabla\Psi(\mathbf{x}) = \mathbf{0}$. Thus, when the network is perturbed, the energy function $\Psi(\mathbf{x})$ monotonically decreases as the system evolves, and becomes constant again only when the system reaches an equilibrium point of Eq. (3) [and hence of Eq. (2)]. Such equilibria represent stable steady states, where the generators are synchronized [$\omega_1(t) = \omega_2(t) = \dots = \omega_{n_g}(t)$], the angle differences are fixed for all pairs of nodes, and the flow is below capacity for all operating transmission lines.

We first illustrate our formalism on Iceland's power-grid network, shown in Fig. 2(a) (for parameter setting, see Supplemental Material [34]). The system is designed to have a stable steady state with no additional failures when any single transmission line is missing (provided

the network remains connected), which is verified in our simulations. We test whether such a cascade-free steady state is actually reached following the removal of a line when the *transient dynamics* between steady states represented in our model is taken into consideration. Starting from the stable steady state determined by Eq. (2), we simulate all 68 single-line removal perturbations that keep the network topologically connected (performed by changing η_ℓ to $\eta_\ell^{(f)}$). Of these, 10 do not converge to the best available stable steady state and instead undergo subsequent failures (Fig. S3 in Supplemental Material [34]). Insights into the underlying mechanism are provided by the example shown in Figs. 2(a)-2(c), where a sequence of line overloads separates the network into 5 clusters. As shown in Fig. 2(d), the system would eventually have approached the designed steady state with no additional failures, but a line overload—whose automatic switch-off triggers subsequent overloads—occurs before the system can reach that state. In this case, no feasible trajectory exists in the phase space connecting the initial state to the steady state predicted by quasi-steady-state models. This scenario is common in general, as shown for five other systems in the 3rd column of Table S2 (Supplemental Material [34]).

When the network is subject to multiple perturbations, our framework shows that the cascade outcome will generally depend on the order and timing of the perturbations. A natural measure to quantify this difference is the size C' (i.e., number of nodes) of the largest connected cluster in the postcascade stable state. As an illustration, we consider the following three scenarios for two-line removal perturbations: (i) remove line $\ell_{i_1-j_1}$ and then, after the stable state is reached, remove line $\ell_{i_2-j_2}$; (ii) same as in (i) but for $\ell_{i_1-j_1}$ swapped with $\ell_{i_2-j_2}$; (iii) remove $\ell_{i_1-j_1}$ and $\ell_{i_2-j_2}$ concurrently. Considering all 2,117 pairs of lines ($\ell_{i_1-j_1}, \ell_{i_2-j_2}$) that keep Iceland's network connected after their removal (but not necessarily after the resulting cascading failures), our simulations indicate that 30.0% of these perturbations lead to cascades in at least one of the scenarios above. For this subset of line pairs, we obtain that: (a) “order matters” in 27.9% of the cases, in that C' differs for at least one of the scenarios; (b) choosing between the orders in (i) and (ii) leads to the largest C' in 20.8% of the cases; (c) (i) and (ii) lead to equally best C' in 4.3% of the cases; (d) the concurrent removal scenario (iii) trumps (i) and (ii) in the remaining 2.8% of the cases (for specific examples, see Figs. S4 and S5 in Supplemental Material [34]). Similar trends are observed for all five other systems considered, as shown in Table S2 (Supplemental Material [34]). This order dependence has potential implications for control, as it can be exploited in proactive line removals to prevent subsequent failures (Fig. S6 in Supplemental Material [34]). This reveals a sharp contrast between processes for which order is immaterial, such as percolation, and the cascades considered here.

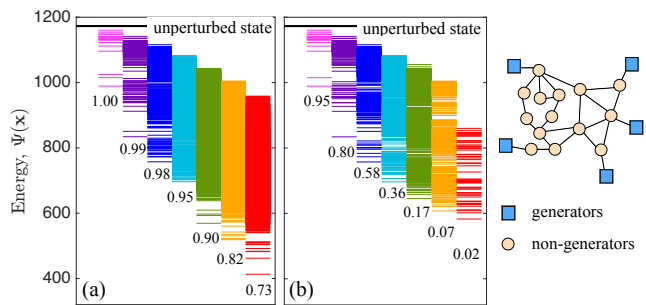


Figure 3. Energy levels $\Psi(\mathbf{x})$ of the stable states in the 14-bus test system. Each panel shows all combinations of 1 (left column) to 7 (right) successive line removals that leave the network connected. (a) All stable states without additional failures determined using the MATLAB function *fsolve*. (b) Subset of stable states in (a) that the system actually evolves to for the same line removals as in (a). Also marked are the fractions of perturbations for which a stable state is identified (a) and the fractions of those stable states actually reached (b). The diagram on the rhs shows the topology of the network.

Taking the analysis one step further, our formalism offers unique insight into the relation between line removal perturbations and energy levels. Figure 3(a) shows all energy levels for stable steady states of the IEEE 14-bus test system (chosen in place of Iceland's network to avoid a cluttered picture) for all combinations of 1 to 7 line removals that keep the network connected. Figure 3(b) shows the states that the system actually approaches following these successive line removals—the missing states [compared to Fig. 3(a)] are the ones not reached because the system undergoes a cascade.

Two major results follow from this. First, it confirms that upon perturbation the system often does not reach the available stable steady state with smallest number of failures (e.g., for 7 line removals, this is so for 98% of all cases). Second, the range of energy levels with $k + 1$ line removals overlaps with the range for k line removals. There are, for example, stable steady states with only one line failure at lower energy than many stable states with 2, 3, ..., 6 line failures. This shows that, following a perturbation that could eventually lead to a stable state with multiple failures, the system can in principle be steered to a lower-energy state which has, nevertheless, a reduced number of failures. Crucially, this is possible without an external input of energy, as the system tends to go spontaneously to lower-energy states following a perturbation.

In summary, the model presented here accounts—for in a single phase space—for the interaction between the full dynamics of a cascade (including transients) and the changes to the underlying network structure imposed by the resulting failures. The results explain the combinatorial impact of perturbations, identify conditions under which a cascade may develop despite the presence of a stable state that would withstand the perturbation, and

suggest new opportunities for cascade control.

The authors thank Takashi Nishikawa for feedback on the manuscript. This work was supported by an ISEN Booster Award, NSF Grant DMS-1057128, Simons Foundation Award 342906, and ARPA-E Award de-ar0000702. The views and opinions of authors expressed herein do not necessarily state or reflect those of the United States Government or any agency thereof.

-
- [1] A. E. Motter and Y. Yang, *Physics Today* **70**(1), 32 (2017).
- [2] R. Liscouski, *et al.*, Final Report on the August 14, 2003 Blackout in the United States and Canada: Causes and Recommendations (2004).
- [3] F. Vandenbergh, *et al.*, Final Report of the Investigation Committee on the 28 September 2003 Blackout in Italy (2004).
- [4] J. A. Dunne and R. J. Williams, *Philos. T. R. Soc. B* **364**, 1711 (2009).
- [5] S. Sahasrabudhe and A. E. Motter, *Nature Commun.* **2**, 170 (2011).
- [6] P. Gai and S. Kapadia, *Proc. Roy. Soc. A* **466**, 2401 (2010).
- [7] M. Elliott, B. Golub, and M. O. Jackson, *Am. Econ. Rev.* **104**, 3115 (2014).
- [8] D. J. Watts, *Proc. Natl. Acad. Sci. U.S.A.* **99**, 5766 (2002).
- [9] A. E. Motter and Y.-C. Lai, *Phys. Rev. E* **66**, 065102(R) (2002).
- [10] K.-I. Goh, D.-S. Lee, B. Kahng, and D. Kim, *Phys. Rev. Lett.* **91**, 148701 (2003).
- [11] P. Crucitti, V. Latora, and M. Marchiori, *Phys. Rev. E* **69**, 045104 (2004).
- [12] S. V. Buldyrev, R. Parshani, G. Paul, H. E. Stanley, and S. Havlin, *Nature* **464**, 1025 (2010).
- [13] C. D. Brummitt, G. Barnett, and R. M. D’Souza, *J. R. Soc. Interface* **12**, 20150712 (2015).
- [14] C. D. Brummitt, R. M. D’Souza, and E. A. Leicht, *Proc. Natl. Acad. Sci. U.S.A.* **109**, E680 (2012).
- [15] A. E. Motter, *Phys. Rev. Lett.* **93**, 098701 (2004).
- [16] I. Dobson, B. A. Carreras, V. E. Lynch, and D. E. Newman, *Chaos* **17**, 026103 (2007).
- [17] M. Anghel, K. A. Werley, and A. E. Motter, *Proc. 40th Ann. HICSS (IEEE, New York, 2007)*, Vol. 1, p. 113.
- [18] D. Watts and H. Ren, *Proc. 2008 IEEE Int. Conf. Sustain. Energy Tech. (IEEE, New York, 2008)*, p. 1200.
- [19] R. D. Zimmerman, C. E. Murillo-Sanchez, and R. J. Thomas, *IEEE T. Power Syst.* **26**, 12 (2011).
- [20] D. Witthaut, M. Rohden, X. Zhang, S. Hallerberg, and M. Timme, *Phys. Rev. Lett.* **116**, 138701 (2016).
- [21] A. Moussawi, N. Derzsy, X. Lin, B. K. Szymanski, and G. Korniss, *Sci. Rep.* **7**, 11729 (2017).
- [22] Y. Susuki, I. Mezić, and T. Hikiyara, *J. Nonlin. Sci.* **21**, 403 (2011).
- [23] M. Rohden, A. Sorge, M. Timme, and D. Witthaut, *Phys. Rev. Lett.* **109**, 064101 (2012).
- [24] A. E. Motter, S. A. Myers, M. Anghel, and T. Nishikawa, *Nature Phys.* **9**, 191 (2013).
- [25] F. Dörfler, M. Chertkov, and F. Bullo, *Proc. Natl. Acad. Sci. U.S.A.* **110**, 2005 (2013).
- [26] P. J. Menck, J. Heitzig, J. Kurths, and H. J. Schellnhuber, *Nature Commun.* **5**, 3969 (2014).
- [27] Theoretical understanding is especially needed given that available reports of empirical data on cascade blackouts generally do not include detailed information about generator behavior along with power flow information.
- [28] A. R. Bergen and D. J. Hill, *IEEE T. Power Ap. Syst.* **PAS-100**, 25 (1981).
- [29] A. Pai, *Energy Function Analysis for Power System Stability* (Springer, 2012).
- [30] C. L. DeMarco, *IEEE Contr. Syst. Mag.* **21**, 40 (2001).
- [31] I. Simonsen, L. Buzna, K. Peters, S. Bornholdt, and D. Helbing, *Phys. Rev. Lett.* **100**, 218701 (2008).
- [32] S.P. Cornelius, W.L. Kath, and A.E. Motter, *Nature Commun.* **4**, 1942 (2013).
- [33] B. Schäfer, D. Witthaut, M. Timme, and V. Latora, *arXiv:1707.08018 [nlin.AO]* (2017).
- [34] See Supplemental Material [url], which includes Refs. [35, 36], for details of the analysis and additional examples.
- [35] H. Zheng and C. L. DeMarco, *Proc. North American Power Symposium, 2010 (IEEE, New York, 2010)*, p. 1.
- [36] F. Milano, An open source power system analysis toolbox, *IEEE T. Power Syst.* **20**, 1199 (2005).
- [37] T. Nishikawa and A. E. Motter, *New J. Phys.* **17**, 015012 (2015).
- [38] These equations follow from Newton’s second law applied to the generator rotor [39]: $I_i \dot{\omega}_i = -\bar{D}_i \omega_i + (\mathcal{T}_i^{(m)} - \mathcal{T}_i^{(e)})$, where I_i is the moment of inertia, \bar{D}_i is the damping coefficient, $\mathcal{T}_i^{(m)}$ is the mechanical torque, and $\mathcal{T}_i^{(e)}$ is the torque due to electrical load in the network. Thus, $M_i = (\omega_o/P_o)I_i$, $D_i = (\omega_o/P_o)\bar{D}_i$, $P_i^{(m)} = [(\omega_i + \omega_o)/P_o]\mathcal{T}_i^{(m)}$, and $\sum_{j=n_g+1}^{n_g+n} \tilde{B}_{ij} \sin \delta_{ij} = [(\omega_i + \omega_o)/P_o]\mathcal{T}_i^{(e)}$, where the relative frequency ω_i is assumed to be small compared to the nominal frequency ω_o , and the base power P_o is used to transform the power terms into per unit quantities.
- [39] J. J. Grainger and W. D. Stevenson, *Power System Analysis* (McGraw-Hill, 1994).
- [40] Iceland’s transmission network, www.maths.ed.ac.uk/optenergy/NetworkData/howtouse.html (accessed: 2016-05-18).

SUPPLEMENTAL MATERIAL

Cascading Failures as Continuous Phase-Space Transitions
 Yang Yang and Adilson E. Motter

DERIVATION OF EQUATION (2) IN THE MAIN TEXT

In a power-grid network, we define a nongenerator node as a bus and transmission lines as electrical connections, including transformers, between pairs of such nodes. We denote the number of nongenerator nodes by n , the number of generators by n_g , and the number of transmission lines by n_l . The operating condition of the network can be characterized by the complex electrical power $S_i^{(e)} = P_i^{(e)} + jQ_i^{(e)}$ at each node i . In steady state, all generators in an alternating current network run at the same frequency and the distribution of power flows through the network is determined by the complex voltage $V_i = |V_i|e^{j\delta_i}$ at each node i , where δ_i is the voltage angle in the reference frame. This is determined through the power flow equations:

$$P_i^{(e)} = \sum_{j=1}^n |V_i||V_j|(G_{ij} \cos \delta_{ij} + B_{ij} \sin \delta_{ij}), \quad (S1)$$

$$Q_i^{(e)} = - \sum_{j=1}^n |V_i||V_j|(G_{ij} \sin \delta_{ij} - B_{ij} \cos \delta_{ij}), \quad (S2)$$

where $\delta_{ij} = \delta_i - \delta_j$ and $Y_{ij} = G_{ij} + jB_{ij}$ define a Laplacian-like matrix. In this matrix, an off-diagonal element Y_{ij} is the negative of the admittance of the line ℓ_{i-j} that connects nodes i and j . Assuming that $|V_i| \approx 1$ p.u. for all nodes and that there is no real power lost on the transmission lines (i.e., $G_{ij} = 0$), we can rewrite the real power as $P_i^{(e)} = \sum_{j=1}^n B_{ij} \sin(\delta_i - \delta_j)$, where B is a symmetric matrix with off-diagonal elements $B_{ij} = -1/x_\ell$ and x_ℓ is the reactance of line ℓ . These assumptions are valid throughout this paper.

In general, the state of both generators and loads can change in time. During a disturbance, the generator rotors decelerate or accelerate with respect to the nominal frequency (60 Hz in the U.S. and 50 Hz in Europe, including Iceland). The dynamics of the generator rotor is governed by the swing equation: $M_i \frac{d\omega_i}{dt} + D_i \omega_i = P_i^{(m)} - P_i^{(e)}$, where ω_i is the frequency (relative to the nominal frequency), M_i is the rotor inertia, D_i is the rotor damping ratio, and $P_i^{(m)}$ is the net shaft power input into the generator. Considering Eq. (S1), we can combine the power flow equations into the swing equation as

$$M_i \frac{d\omega_i}{dt} + D_i \omega_i = P_i^{(m)} - \sum_{j=1}^n B_{ij} \sin(\delta_i - \delta_j). \quad (S3)$$

Here we choose the angle of the first generator as the reference angle, and we define $\delta_i = \alpha_i - \alpha_1$, where $\frac{d\alpha_i}{dt} = \omega_i$. In principle, the power consumed by load nodes could depend nonlinearly on the frequency at that node. Assuming that the frequency at each node does not deviate strongly from the nominal frequency, we can use a linearized power-frequency relation to describe the dynamics of the node connected with a load:

$$T_i \frac{d\delta_i}{dt} = P_i^{(d)} - \sum_{j=1}^n B_{ij} \sin(\delta_i - \delta_j) - \omega_i, \quad (S4)$$

where T_i is a positive constant and $P_i^{(d)}$ is the power requested by the load.

To account for the internal reactances of the generators, we adopted an extended representation of the power grid. As explained in the main text, in this extended representation we add n_g nodes connected to the network through virtual lossless lines to represent the n_g generators in the system (see Fig. S2). The reactance of a virtual line represents the transient reactance of the corresponding generator. Accordingly, we modify the B matrix in Eqs. (S3) and (S4) as

$$\tilde{B} = \begin{bmatrix} 0 & X \\ X^T & B \end{bmatrix}, \quad (S5)$$

where X_{ij} is the reciprocal of the transient reactance of the i th generator that connects the j th node in the network. Combining together the dynamics of generators and loads, the equations of motion take the following form:

$$\begin{aligned} M_i \frac{d\omega_i}{dt} + D_i \omega_i &= P_i^{(m)} - \sum_{j=1}^{n_g+n} \tilde{B}_{ij} \sin(\delta_i - \delta_j), & i = 1, 2, \dots, n_g, \\ \frac{d\delta_i}{dt} &= \omega_i - \omega_1, & i = 2, \dots, n_g, \\ T_i \frac{d\delta_i}{dt} &= -P_i^{(d)} - \sum_{j=1}^{n_g+n} \tilde{B}_{ij} \sin(\delta_i - \delta_j) - \omega_1, & i = n_g + 1, \dots, n_g + n, \end{aligned} \quad (S6)$$

where, for simplicity, the last equation is assumed to apply to all nongenerator nodes under the assumption that they all include some frequency-dependent power exchange. Adding up all the equations in Eq. (S6), at the fixed point of the dynamics (where $d\omega_i/dt = 0$, $d\delta_i/dt = 0$) we obtain $(\sum_{i=1}^{n_g} D_i + n)\omega_1 = \sum_{i=1}^{n_g} P_i^{(m)} - \sum_{n_g+1}^{n_g+n} P_i^{(d)}$. We assume that the real power is balanced, i.e., $\sum_{i=1}^{n_g} P_i^{(m)} = \sum_{n_g+1}^{n_g+n} P_i^{(d)}$, and hence all generators operate with the nominal frequency at the fixed point.

To complete the derivation of Eq. (2), for each transmission line ℓ_{i-j} we need to define the fraction $\lambda_{\ell_{i-j}}$ of the line capacity used by the flow. This quantity is determined by the average amount of reactive power stored in the transmission line, calculated as $\frac{1}{2}|(V_i - V_j)I_{ij}^*|$, where $I_{ij} = j B_{ij}(V_i - V_j)$ is the current on the line. Noting that $|V_i| \approx |V_j|$ (both approximately equal to 1 p.u.), we can determine this reactive energy as $\tilde{B}_{ij}(1 - \cos \delta_{ij})$, and replace $\lambda_{\ell_{i-j}}$ in Eq. (1) by this reactive energy divided by $W_{\ell_{i-j}}$ (the maximum reactive energy that line ℓ_{i-j} can hold). By incorporating the dynamics of the status variables, as presented in the main text, into the dynamics of the power system in Eq. (S6), we finally obtain Eq. (2). This equation describes, at the same time, the state variables of the power system and the status of the transmission lines.

PROOF OF EQUATION (3) IN THE MAIN TEXT

We now explicitly show the equivalence between Eqs. (3) and (2) in the main text. We recall that the state of a power system is defined as $\mathbf{x} = (\boldsymbol{\omega}, \boldsymbol{\delta}, \boldsymbol{\eta})$. As in the main text, the (relative) frequencies of the generators are represented by a vector $\boldsymbol{\omega}$ of size $n_g \times 1$, the phase angles of all nodes relative to the reference node are represented by a vector $\boldsymbol{\delta}$ of size $(n_g + n - 1) \times 1$, and the status variables of the transmission lines are represented by a vector $\boldsymbol{\eta}$ of size $n_l \times 1$. To facilitate our verification of Eq. (3), we further separate $\boldsymbol{\delta}$ into $\boldsymbol{\delta} = (\boldsymbol{\delta}', \boldsymbol{\delta}'')$, where the vector $\boldsymbol{\delta}' = (\delta_2, \dots, \delta_{n_g})$ represents the phase angles of the generator nodes and vector $\boldsymbol{\delta}'' = (\delta_{n_g+1}, \dots, \delta_{n_g+n})$ represents the phase angles of nongenerator nodes.

According to Eq. (4), the gradient of $\Psi(\mathbf{x})$ can be decomposed as $\nabla \Psi(\mathbf{x}) = [\nabla_{\boldsymbol{\omega}} \Psi(\mathbf{x}), \nabla_{\boldsymbol{\delta}'} \Psi(\mathbf{x}), \nabla_{\boldsymbol{\delta}''} \Psi(\mathbf{x}), \nabla_{\boldsymbol{\eta}} \Psi(\mathbf{x})]$, where

$$\nabla_{\boldsymbol{\omega}} \Psi(\mathbf{x}) = [M_1 \omega_1, M_2 \omega_2, \dots, M_{n_g} \omega_{n_g}]^T, \quad (S7)$$

$$\nabla_{\boldsymbol{\delta}'} \Psi(\mathbf{x}) = \begin{bmatrix} \sum_{j=1}^{n_g+n} \tilde{B}_{2j} \sin \delta_{2j} + P_2 \\ \sum_{j=1}^{n_g+n} \tilde{B}_{3j} \sin \delta_{3j} + P_3 \\ \vdots \\ \sum_{j=1}^{n_g+n} \tilde{B}_{n_g j} \sin \delta_{n_g j} + P_{n_g} \end{bmatrix}, \quad (S8)$$

$$\nabla_{\boldsymbol{\delta}''} \Psi(\mathbf{x}) = \begin{bmatrix} \sum_{j=1}^{n_g} \tilde{B}_{(n_g+1)j} \sin \delta_{(n_g+1)j} + \sum_{j=n_g+1}^{n_g+n} \tilde{B}_{(n_g+1)j} \sin \delta_{(n_g+1)j} \eta_{\ell_{(n_g+1)-j}} + P_{n_g+1} \\ \sum_{j=1}^{n_g} \tilde{B}_{(n_g+2)j} \sin \delta_{(n_g+2)j} + \sum_{j=n_g+1}^{n_g+n} \tilde{B}_{(n_g+2)j} \sin \delta_{(n_g+2)j} \eta_{\ell_{(n_g+2)-j}} + P_{n_g+2} \\ \vdots \\ \sum_{j=1}^{n_g} \tilde{B}_{(n_g+n)j} \sin \delta_{(n_g+n)j} + \sum_{j=n_g+1}^{n_g+n} \tilde{B}_{(n_g+n)j} \sin \delta_{(n_g+n)j} \eta_{\ell_{(n_g+n)-j}} + P_{n_g+n} \end{bmatrix}, \quad (S9)$$

$$\nabla_{\boldsymbol{\eta}}\Psi(\mathbf{x}) = \begin{bmatrix} \vdots \\ \tilde{B}_{ij}(1 - \cos \delta_{ij}) - W_{\ell_{i-j}} f(\eta_{\ell_{i-j}}) \\ \vdots \end{bmatrix}. \quad (\text{S10})$$

In the last equation, each component of $\nabla_{\boldsymbol{\eta}}\Psi(\mathbf{x})$ corresponds to the derivative of $\Psi(\mathbf{x})$ with respect to the status variable of a transmission line ℓ_{i-j} . For notational convenience, in the expression of $\nabla_{\boldsymbol{\delta}'}\Psi(\mathbf{x})$ we introduce the constants $\eta_{\ell_{(n_g+i)-j}} \equiv 0$ associated with pairs of nodes $(n_g + i, j)$ that are not connected by a transmission line (these constants should not be confused with the components of $\boldsymbol{\eta}$, which are variables associated with pairs of nodes that are connected).

Making use of the definition of matrix J in Eqs. (5)-(7) of the main text, we obtain

$$\begin{aligned} J_{11}\nabla_{\boldsymbol{\omega}}\Psi(\mathbf{x}) + J_{12}\nabla_{\boldsymbol{\delta}'}\Psi(\mathbf{x}) + J_{13}\nabla_{\boldsymbol{\delta}''}\Psi(\mathbf{x}) &= \begin{bmatrix} \frac{-D_1}{M_1}\omega_1 \\ \frac{-D_2}{M_2}\omega_2 \\ \vdots \\ \frac{-D_{n_g}}{M_{n_g}}\omega_{n_g} \end{bmatrix} + \begin{bmatrix} \frac{1}{M_1} \sum_{i=2}^{n_g} (\sum_{j=1}^{n_g+n} \tilde{B}_{ij} \sin \delta_{ij} + P_i) \\ \frac{-1}{M_2} (\sum_{j=1}^{n_g+n} \tilde{B}_{2j} \sin \delta_{2j} + P_2) \\ \vdots \\ \frac{-1}{M_{n_g}} (\sum_{j=1}^{n_g+n} \tilde{B}_{2j} \sin \delta_{n_g j} + P_{n_g}) \end{bmatrix} \\ &+ \begin{bmatrix} \frac{1}{M_1} \sum_{i=n_g+1}^{n_g+n} (\sum_{j=1}^{n_g} \tilde{B}_{ij} \sin \delta_{ij} + \sum_{j=n_g+1}^{n_g+n} \tilde{B}_{ij} \sin \delta_{ij} \eta_{\ell_{i-j}} + P_i) \\ 0 \\ \vdots \\ 0 \end{bmatrix}. \end{aligned} \quad (\text{S11})$$

We note that $\sum_{i=n_g+1}^{n_g+n} \sum_{j=n_g+1}^{n_g+n} \tilde{B}_{ij} \sin \delta_{ij} \eta_{\ell_{i-j}} = 0$ given that $\tilde{B}_{ij} = \tilde{B}_{ji}$ and $\sin \delta_{ij} = -\sin \delta_{ji}$. Accordingly, the first row of the rhs of Eq. (S11) can be rewritten as

$$\begin{aligned} &-\frac{D_1}{M_1}\omega_1 + \frac{1}{M_1} (\sum_{i=2}^{n_g} \sum_{j=1}^{n_g+n} \tilde{B}_{ij} \sin \delta_{ij} + \sum_{i=n_g+1}^{n_g+n} \sum_{j=1}^{n_g} \tilde{B}_{ij} \sin \delta_{ij}) + \frac{1}{M_1} \sum_{i=2}^{n_g+n} P_i \\ &= -\frac{D_1}{M_1}\omega_1 + \frac{1}{M_1} (\sum_{i=2}^{n_g} \sum_{j=1}^{n_g+n} \tilde{B}_{ij} \sin \delta_{ij} + \sum_{i=n_g+1}^{n_g+n} \sum_{j=1}^{n_g} \tilde{B}_{ij} \sin \delta_{ij}) - \frac{1}{M_1} P_1 \\ &= -\frac{D_1}{M_1}\omega_1 + \frac{1}{M_1} (\sum_{i=2}^{n_g} \sum_{j=1}^{n_g+n} \tilde{B}_{ij} \sin \delta_{ij} + \sum_{j=n_g+1}^{n_g+n} \sum_{i=1}^{n_g} \tilde{B}_{ji} \sin \delta_{ji}) - \frac{1}{M_1} P_1 \\ &= -\frac{D_1}{M_1}\omega_1 + \frac{1}{M_1} (\sum_{i=2}^{n_g} \sum_{j=1}^{n_g+n} \tilde{B}_{ij} \sin \delta_{ij} - \sum_{j=n_g+1}^{n_g+n} \sum_{i=1}^{n_g} \tilde{B}_{ij} \sin \delta_{ij}) - \frac{1}{M_1} P_1 \\ &= -\frac{D_1}{M_1}\omega_1 + \frac{1}{M_1} (\sum_{i=2}^{n_g} \sum_{j=1}^{n_g+n} \tilde{B}_{ij} \sin \delta_{ij} - \sum_{j=1}^{n_g+n} \sum_{i=1}^{n_g} \tilde{B}_{ij} \sin \delta_{ij}) - \frac{1}{M_1} P_1 \\ &= -\frac{D_1}{M_1}\omega_1 - \frac{1}{M_1} \sum_{j=1}^{n_g+n} \tilde{B}_{ij} \sin \delta_{ij} - \frac{1}{M_1} P_1. \end{aligned} \quad (\text{S12})$$

In the above derivation, we assume that the total amount of power injection into the network equals the total amount of power extracted from the network (i.e., $\sum_{i=1}^{n_g+n} P_i = 0$), and we use the fact that $\tilde{B}_{ij} = 0$ for $i, j = 1, 2, \dots, n_g$. Similar calculation applies to the other rows of Eq. (S11). Then, noting that the rhs of Eq. (S11) is the same as the rhs of the first equation in (2), we conclude that $J_{11}\nabla_{\boldsymbol{\omega}}\Psi(\mathbf{x}) + J_{12}\nabla_{\boldsymbol{\delta}'}\Psi(\mathbf{x}) + J_{13}\nabla_{\boldsymbol{\delta}''}\Psi(\mathbf{x}) = \frac{d\boldsymbol{\omega}}{dt}$.

Next, we establish the equivalence between the other components of Eq. (3) and the other equations in (2). We obtain the second equation in (2) using that

$$-J_{12}^T \nabla_{\boldsymbol{\omega}}\Psi(\mathbf{x}) = \begin{bmatrix} \omega_2 - \omega_1 \\ \omega_3 - \omega_1 \\ \vdots \\ \omega_{n_g} - \omega_1 \end{bmatrix} = \frac{d\boldsymbol{\delta}'}{dt}, \quad (\text{S13})$$

the third equation in (2) using that

$$\begin{aligned}
& -J_{13}^T \nabla_{\boldsymbol{\omega}} \Psi(\mathbf{x}) + J_{33} \nabla_{\boldsymbol{\delta}} \Psi(\mathbf{x}) = \\
& \begin{bmatrix} -\omega_1 \\ -\omega_1 \\ \vdots \\ -\omega_1 \end{bmatrix} + \begin{bmatrix} -\frac{1}{T_{n_g+1}} \left(\sum_{j=1}^{n_g} \tilde{B}_{(n_g+1)j} \sin \delta_{(n_g+1)j} + \sum_{j=n_g+1}^{n_g+n} \tilde{B}_{(n_g+1)j} \sin \delta_{(n_g+1)j} \eta_{\ell_{(n_g+1)-j}} + P_{n_g+1} \right) \\ -\frac{1}{T_{n_g+2}} \left(\sum_{j=1}^{n_g} \tilde{B}_{(n_g+2)j} \sin \delta_{(n_g+2)j} + \sum_{j=n_g+1}^{n_g+n} \tilde{B}_{(n_g+2)j} \sin \delta_{(n_g+2)j} \eta_{\ell_{(n_g+2)-j}} + P_{n_g+2} \right) \\ \vdots \\ -\frac{1}{T_{n_g+n}} \left(\sum_{j=1}^{n_g} \tilde{B}_{(n_g+n)j} \sin \delta_{(n_g+n)j} + \sum_{j=n_g+1}^{n_g+n} \tilde{B}_{(n_g+n)j} \sin \delta_{(n_g+n)j} \eta_{\ell_{(n_g+n)-j}} + P_{n_g+n} \right) \end{bmatrix} \\
& = \frac{d\boldsymbol{\delta}''}{dt}, \tag{S14}
\end{aligned}$$

and the fourth equation in (2) using that

$$J_{44} \nabla_{\boldsymbol{\eta}} \Psi(\mathbf{x}) = \begin{bmatrix} \vdots \\ -\frac{\tilde{B}_{ij}(1 - \cos \delta_{ij})}{W_{\ell_{i-j}}} + f(\eta_{\ell_{i-j}}) \\ \vdots \end{bmatrix} = \frac{d\boldsymbol{\eta}}{dt}. \tag{S15}$$

Combining Eqs. (S11)-(S15), we have proved Eq. (3) in the main text. We note that a similar result on a 3-bus network is reported in Ref. [35]. However, that study does not offer a framework to address a network with an arbitrary number of buses, which is derived here.

For completeness, we note that our energy-function formulation is also naturally suited for stability analysis. Rewriting Eq. (3) as $\dot{\mathbf{x}} = \mathbf{g}(\mathbf{x})$, if \mathbf{x}^* is an equilibrium state, by definition we have $\mathbf{g}(\mathbf{x}^*) = \mathbf{0}$. The stability of this state is then determined by the eigenvalues of the Jacobian matrix $d\mathbf{g}/d\mathbf{x}|_{\mathbf{x}=\mathbf{x}^*} = JH(\mathbf{x}^*)$, where the components of matrix H are given by $H_{kk'} = \frac{\partial^2 \Psi}{\partial x_k \partial x_{k'}}$.

GENERALIZED HAMILTONIAN-LIKE ENERGY WHEN THE NETWORK SPLITS

Our analysis of the energy function $\Psi(\mathbf{x})$ assumes a balance of power in the network, which is guaranteed when the network remains connected but can be violated when it splits during a cascade. This is easily remediated, however, by extending the formalism to introduce a reference generator in each cluster to mimic the system's operation of rebalancing real power. As shown below, the reference generator in each cluster then serves as a slack bus that prevents imbalances between power input and output, which would cause acceleration or deceleration of generators. In our applications in the paper, the network remains connected or else we consider each cluster separately.

We first note that the choice of the reference generator does not impact our description of power-grid dynamics, as long as the power input and output at each node is fixed. Then we can show that in a power network satisfying $\sum_{i=1}^{n_g+n} P_i = 0$, the value of the energylike function $\Psi(\mathbf{x})$ remains the same for different choices of the reference node. Specifically, when the angle of generator 1 is chosen to be the reference, the state is originally defined as $\mathbf{x} = (\boldsymbol{\omega}, \boldsymbol{\delta}, \boldsymbol{\eta})$, where the frequency is defined by $\omega_i = \frac{d\alpha_i}{dt}$, the reference angle is defined by $\boldsymbol{\delta} = (\delta_2, \delta_3, \dots, \delta_{n_g}) \equiv (\alpha_2 - \alpha_1, \alpha_3 - \alpha_1, \dots, \alpha_{n_g} - \alpha_1)$, and α_i is the phase angle of node i . Here, if we change the reference node to be node r , the state vector needs to be redefined as $\mathbf{x}^{(r)} = (\boldsymbol{\omega}, \boldsymbol{\delta}^{(r)}, \boldsymbol{\eta})$, where

$$\boldsymbol{\delta}^{(r)} = (\delta_1^{(r)}, \delta_2^{(r)}, \dots, \delta_{r-1}^{(r)}, \delta_{r+1}^{(r)}, \dots, \delta_{n_g+n}^{(r)}) \equiv (\alpha_1 - \alpha_r, \alpha_2 - \alpha_r, \dots, \alpha_{r-1} - \alpha_r, \alpha_{r+1} - \alpha_r, \dots, \alpha_{n_g+n} - \alpha_r). \tag{S16}$$

We note that, in the redefined phase space, the angle difference between two nodes remains the same as in the original frame, i.e., $\delta_{ij}^{(r)} \equiv \delta_i^{(r)} - \delta_j^{(r)} = (\alpha_i - \alpha_r) - (\alpha_j - \alpha_r) = \alpha_i - \alpha_j = \delta_i - \delta_j \equiv \delta_{ij}$. Therefore, the energylike function in the new reference frame, which we denote $\Psi(\mathbf{x}^{(r)})$, can be written using the expression in Eq. (4) but with the term

$\sum_{i=2}^{n_g+n} P_i \delta_i$ replaced by $\sum_{\substack{i=1 \\ i \neq r}}^{n_g+n} P_i \delta_i^{(r)}$. By making use of $\sum_{i=1}^{n_g+n} P_i = 0$, we can further derive

$$\sum_{\substack{i=1 \\ i \neq r}}^{n_g+n} P_i \delta_i^{(r)} = \sum_{\substack{i=1 \\ i \neq r}}^{n_g+n} P_i \alpha_i - \left[\sum_{\substack{i=1 \\ i \neq r}}^{n_g+n} P_i \right] \alpha_r = \sum_{\substack{i=1 \\ i \neq r}}^{n_g+n} P_i \alpha_i + P_r \alpha_r = \sum_{i=2}^{n_g+n} P_i \alpha_i + P_1 \alpha_1 = \sum_{i=2}^{n_g+n} P_i \alpha_i - \left[\sum_{i=2}^{n_g+n} P_i \right] \alpha_1 = \sum_{i=2}^{n_g+n} P_i \delta_i. \quad (\text{S17})$$

We can conclude, therefore, that the energy function remains unchanged when we choose a different reference generator node. In the same way we proved Eq. (3), we can also prove that

$$\frac{d\mathbf{x}^{(r)}}{dt} = J^{(r)} \nabla \Psi(\mathbf{x}^{(r)}), \quad (\text{S18})$$

where $J^{(r)}$ is a full-rank matrix of the form

$$J^{(r)} = \begin{bmatrix} J_{11} & J_{12}^{(r)} & J_{13}^{(r)} & \mathbf{0} \\ -[J_{12}^{(r)}]^T & \mathbf{0} & \mathbf{0} & \mathbf{0} \\ -[J_{13}^{(r)}]^T & \mathbf{0} & J_{33} & \mathbf{0} \\ \mathbf{0} & \mathbf{0} & \mathbf{0} & J_{44} \end{bmatrix}. \quad (\text{S19})$$

In this matrix, the off-diagonal blocks are

$$J_{12}^{(r)} = \begin{bmatrix} \frac{-1}{M_1} & 0 & 0 & \dots & \dots & \dots & \dots & 0 \\ 0 & \frac{-1}{M_2} & 0 & \dots & \dots & \dots & \dots & 0 \\ \vdots & \vdots & \ddots & \ddots & \ddots & \ddots & \ddots & \vdots \\ 0 & 0 & \dots & \frac{-1}{M_{r-1}} & 0 & 0 & \dots & 0 \\ \frac{1}{M_r} & \frac{1}{M_r} & \dots & \frac{1}{M_r} & \frac{1}{M_r} & \frac{1}{M_r} & \dots & \frac{1}{M_r} \\ 0 & 0 & \dots & 0 & 0 & \frac{-1}{M_{r+1}} & \dots & 0 \\ \vdots & \vdots & \ddots & \ddots & \ddots & \ddots & \ddots & \vdots \\ 0 & 0 & \dots & \dots & \dots & \dots & \dots & \frac{-1}{M_{n_g}} \end{bmatrix}, \quad J_{13}^{(r)} = \begin{bmatrix} 0 & \dots & 0 \\ \vdots & \vdots & \vdots \\ 0 & \dots & 0 \\ \frac{1}{M_r} & \dots & \frac{1}{M_r} \\ 0 & \dots & 0 \\ \vdots & \vdots & \vdots \\ 0 & \dots & 0 \end{bmatrix}, \quad (\text{S20})$$

where $J_{13}^{(r)}$ is an $n_g \times n$ matrix with nonzero elements in row r , and the diagonal blocks are the same as defined in Eq. (7) of the main text.

To proceed, we consider the situation in which a network G is split into $k \geq 2$ disconnected clusters G_1, \dots, G_k due to line failures. Without loss of generality, we assume that G_1 is the largest cluster in the network and that G_1 contains the reference node r (which can be otherwise reassigned since the choice of the reference node does not impact the dynamics or the value of Ψ). After rebalancing the power input and output in G_1 by setting $\sum_{i \in G_1} P_i = 0$, we can consider the dynamics in the corresponding subspace of the phase space of the system using our formalism:

$$\frac{d\overline{\mathbf{x}}^{(r)}}{dt} = \overline{J}^{(r)} \nabla \Psi(\overline{\mathbf{x}}^{(r)}). \quad (\text{S21})$$

Here, the substate $\overline{\mathbf{x}}^{(r)}$ contains only the variables for the nodes (generators and nongenerators) and transmission lines in the cluster G_1 . The matrix $\overline{J}^{(r)}$ and function $\Psi(\overline{\mathbf{x}}^{(r)})$ are defined on the cluster G_1 in the same way as $J^{(r)}$ and $\Psi(\mathbf{x}^{(r)})$ were defined for the entire network G . The same procedure can be used in each cluster of the network, thereby leading to a self-consistent approach that can be applied to the general case in which the network splits into disconnected clusters during a cascade.

There is an exceptional case under which our formalism will fail. Recalling that P_r is the negative of the mechanical power input from the generator node r , the sum $\sum_{\substack{i \in G_1 \\ i \neq r}} P_i = -P_r$ must be a nonnegative number smaller than the reciprocal of the transient reactance of the generator. The corresponding condition must hold true for each cluster. If for any cluster we are not able to select a reference generator such that this condition is satisfied, we declare it an unsolvable state. This state corresponds to the situation in which we are not able to rebalance the power input and output in a cluster by adjusting the input from any single generator in the cluster, and hence the cascade will necessarily continue to propagate in that cluster. Other operations, such as shedding power and adjusting the input from multiple generators, would be generally needed in this case to rebalance the system.

POWER NETWORK DATA

To the best of our knowledge, this is the first study on power grids to account for both line overload and generator dynamics in the same cascade event. Our analysis requires static power flow data and dynamic data on the parameters of the generators. The power flow data include the graph topology and electrical parameters of the transmission lines as well as the power-demand and generator-output data. The power-grid network of Iceland considered in this work is the largest publicly available system known to us with consistent static and dynamic data, in which the static generator data can be matched to the generator data used in stability tests. This network has the additional advantage of being isolated, and therefore involves no assumptions on possible external connections. The other networks used to complement our analysis are standard test systems often employed in power flow studies. They consist of four IEEE test transmission systems and the PEGASE 89-bus system, which represents a transmission network in Europe available through Matpower 5.0.

Iceland's network is shown in Fig. S3. The static and dynamic parameters of this system are provided in Ref. [40]. The available data include the real power $P_i^{(m)}$ supplied by each generator, the real power $P_i^{(d)}$ demanded at each node, the reactance x_ℓ of each transmission line, and the dynamic data (including rotor inertia M_i and transient reactance) of each generator. We choose the load frequency ratio to be $T_i = 1$ for every nongenerator node and the rotor damping ratio to be $D_i = 5$ for every generator in the network. The assumption that these parameters are the same for the different nodes is not essential; other choices are possible, and are consistent with the mathematical assumptions underlying Eq. (S6) and our formalism, provided that the parameters in the denominators of Eqs. (6) and (7) are nonzero. If there are two lines connecting a pair of nodes, we replace them by a single line with the combined impedance. For one of the lines, whose actual reactance is not available in the data, the reactance is assigned to be 0.0001 p.u. to assure that this line has a large capacity. To define the capacity of each transmission line, we calculate the steady-state power-flow solutions [determined by Eq. (S1)] for all possible one-line failure scenarios that keep the network connected. We then assign the capacity W_ℓ of each line to be 110% of the maximum reactance energy that the line ℓ stores in these solutions. In this way, the system has at least one stable steady state when a transmission line is disconnected (as long as the network remains connected, as assumed).

The basic properties of the test systems are listed in Table S1 [36], where we also include Iceland's network for completeness. In particular, the IEEE 14-bus test system in Fig. 3 consists of 5 generator nodes, 14 nongenerator nodes (i.e., buses), and 20 transmission lines. The information available on these systems includes data on the real power $P_i^{(m)}$ supplied by each generator, the real power $P_i^{(d)}$ requested at each node, and the reactance x_ℓ for each transmission line [36]. In our calculations, we keep all these parameters unchanged except for the $P_i^{(m)}$ of the generators with zero output of real power. To include those generators in our formalism, we assume that they have a small real-power output of 1 MW. We also assume that all generator rotors have identical dynamic parameters, with rotor inertia $M_i = 5$ (in seconds) and rotor damping ratio $D_i = 5$. The transient reactance of each generator is chosen to be 0.001 p.u., which guarantees that the angle difference between the two ends of the line connecting the generator node (and hence instability) remains small during cascades. Finally, the load frequency ratio T_i and line capacities W_ℓ are assigned in the same way as in Iceland's power grid.

Table S1. Description of the power systems used in this work. The columns represent the number of buses (n), generators (n_g), and power lines (n_l), respectively.

Power systems	n	n_g	n_l
IEEE14	14	5	20
IEEE39	39	10	45
IEEE57	57	7	78
PEGASE89	89	12	206
IEEE118	118	54	179
Iceland	189	35	203

Table S2. Cascades triggered by single- and double-line removal perturbations on the test power systems considered. Here, N is the number of perturbations that keep the network initially connected and N_T is the number of such perturbations that trigger cascades. Also shown is the number of double-line removals N^{OM} for which the resulting C' depends on the perturbation schedule (i)-(iii) (defined in the main text), as well as the breakdown into the number for which the largest C' results from either (i) or (ii) (N^{E}), from both (i) and (ii) (N^{B}), and from (iii) (N^{C}). Similar results for Iceland's power grid are presented in the main text.

System	Single		Double					
	N	N_T	N	N_T	N^{OM}	N^{E}	N^{B}	N^{C}
IEEE14	19	1	163	45	17	9	8	0
IEEE39	35	3	562	81	43	27	11	5
IEEE57	77	3	2859	220	83	71	6	6
PEGASE89	189	5	17739	1092	308	245	34	29
IEEE118	170	3	14289	946	564	455	80	29

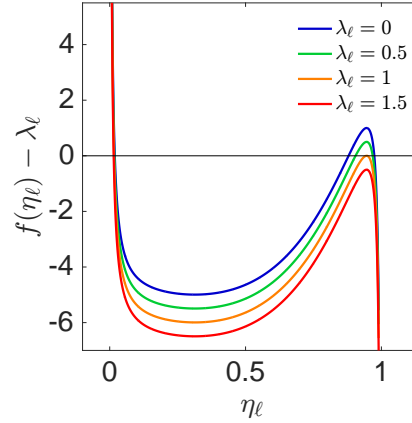


Figure S1. Equivalent of Fig. 1(a) [i.e., the rhs of Eq. (1)] for different values of λ_ℓ .

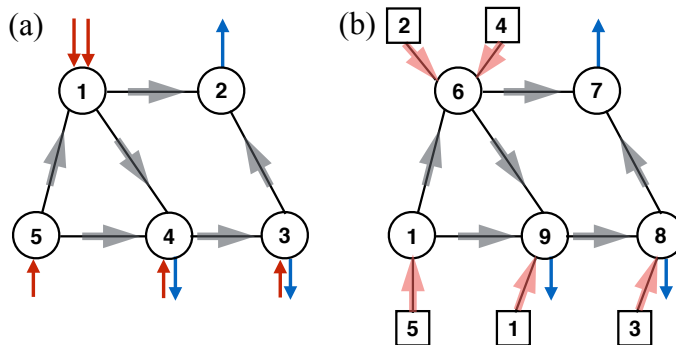


Figure S2. Network representations for a hypothetical 5-bus power system. (a) Original representation, where each node is associated with a load (blue arrow) and/or a redistribution point, which may be connected to one or more generators (red arrows). The wide gray arrows indicate the direction of the flow on the lines. (b) Extended representation, where each generator is modeled as an additional node (square) that injects power into the original network through a virtual line (wide red arrow).

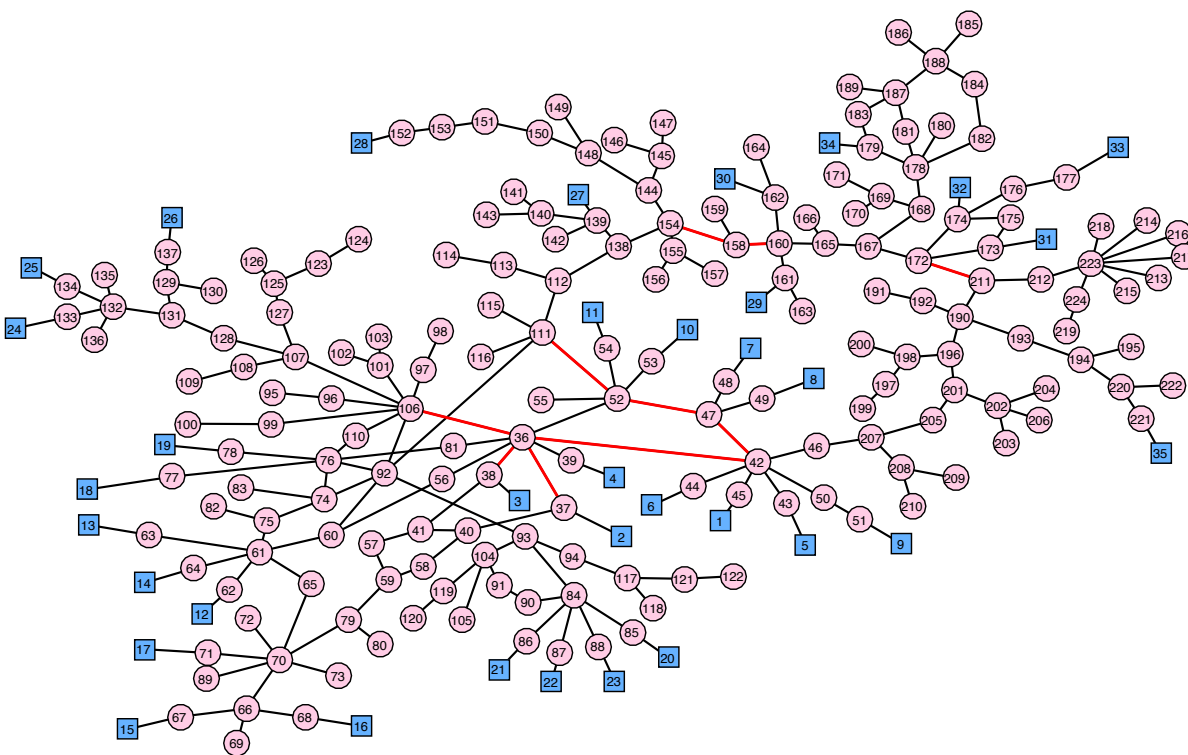


Figure S3. Network representation of Iceland's power-grid system. Generators are indicated by squares and nongenerator nodes by circles. Under the conditions considered here, there are 10 single-line removal perturbations (red) that lead to cascades in this system.

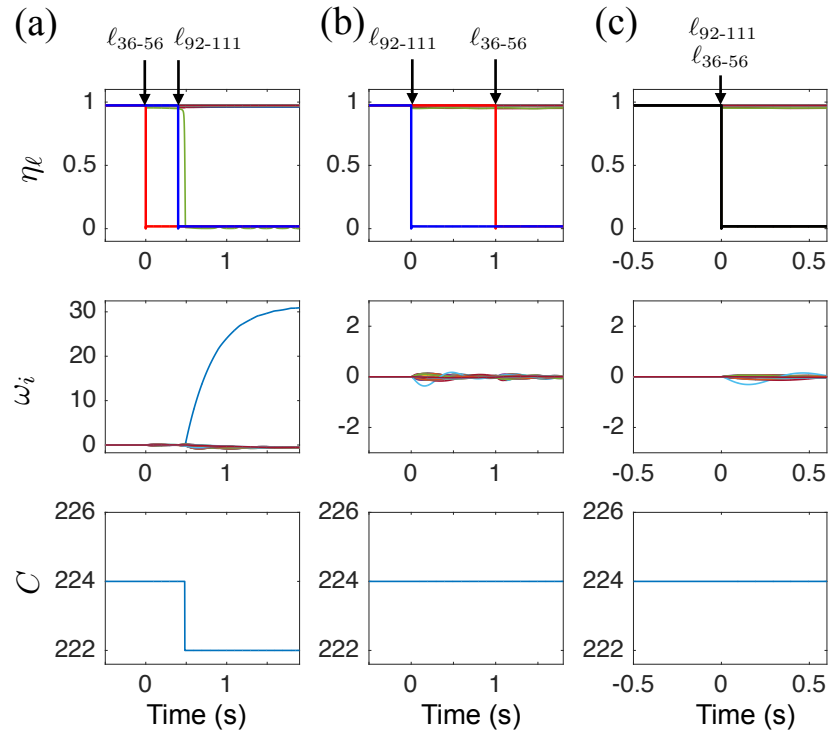


Figure S4. Impact of perturbation order in Iceland's power grid for the removal of lines l_{36-56} and l_{92-111} according to the three scenarios considered in the main text: (a) removal of l_{36-56} followed by the removal of l_{92-111} ; (b) removal of l_{92-111} followed by the removal of l_{36-56} ; (c) concurrent removal of l_{36-56} and l_{92-111} . The dynamics of the power grid is represented by the status of the transmission lines η_ℓ (top panels), the frequency of the generators ω_i (middle panels), and the size of the largest cluster C (bottom panel).

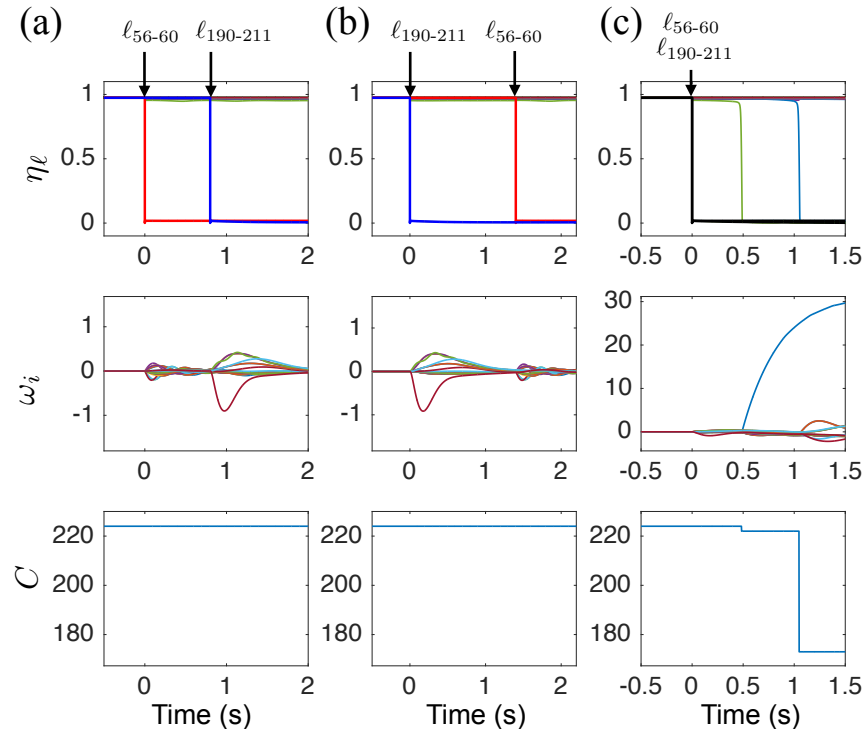


Figure S5. Same as Fig. S4 for the removal of lines l_{56-60} and $l_{190-211}$. In this case the concurrent removal of the two lines has the highest impact, while in the example of Fig. S4 a cascade can only be triggered by the separate removal of the lines.

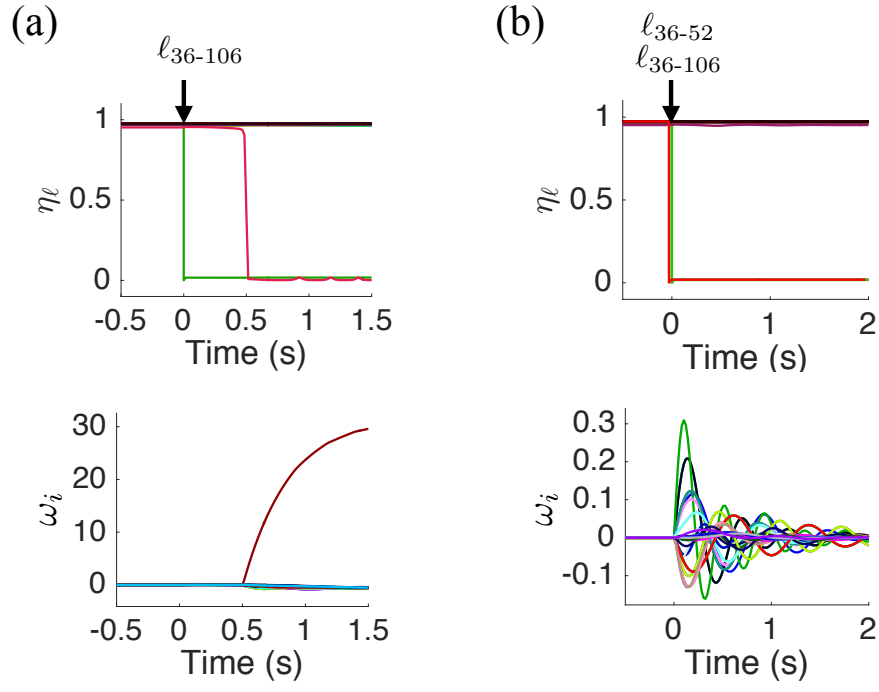


Figure S6. Rescue perturbation in Iceland's power-grid system. (a) The removal of line ℓ_{36-106} eventually leads to the separation of generator 1 due to the overload of line ℓ_{42-45} , which causes the network to lose 189 MW in power generation (13.8% of its total). (b) The concurrent removal of line ℓ_{36-52} along with ℓ_{36-106} prevents subsequent failures and power losses, keeping the network connected. The top panels show the status of the transmission lines η_ℓ and the bottom panels show the frequency of the generators ω_i .